express
polymer letters

Research article

Studies on composite proton exchange membranes made from poly(vinyl alcohol-*co*-styrenesulfonic acid)/non-woven fabric for direct methanol fuel cell

Rikarani R. Choudhury[1] , *Jaydevsinh M. Gohil*[2,3]* , *Akshaya K. Palai*[1] , *Kingshuk Dutta*[2] ,
Smita Mohanty[1]

[1]Laboratory for Advanced Research in Polymeric Materials (LARPM), School for Advanced Research in Petrochemicals (SARP), Central Institute of Petrochemicals Engineering & Technology (CIPET), 751024 Bhubaneswar, Odisha, India
[2]Advanced Polymer Design and Development Research Laboratory (APDDRL), School for Advanced Research in Petrochemicals (SARP), Central Institute of Petrochemicals Engineering and Technology (CIPET), 562149 Bengaluru, Karnataka, India
[3]Advanced Research School for Technology and Product Simulation (ARSTPS), School for Advanced Research in Petrochemicals (SARP), Central Institute of Petrochemicals Engineering and Technology (CIPET), 600032 Chennai, Tamil Nadu, India

Abstract. Various materials have been examined over the last several decades to fabricate proton exchange membranes (PEMs) for direct methanol fuel cells (DMFCs), with the objective of achieving high selectivity (*i.e.*, the ratio of proton conduction to fuel permeability). Ideally, a PEM for DMFC must demonstrate higher proton conductivity, as well as lower methanol permeability, in comparison to the commercial Nafion membranes. With these objectives, this research paper reports the fabrication of a composite PEM comprising glutaraldehyde-crosslinked poly(vinyl alcohol-*co*-styrenesulfonic acid) and sulfonated polypropylene-based non-woven fabric (S-NWF) by deep coating technique. The resulting PEMs were thoroughly characterized to find physicochemical and electrochemical properties. Key findings obtained with these composite PEMs are (a) exhibition of dimensional stability in hot water (at 80 °C), (b) improved proton conductivity (*i.e.*, 0.12 S·cm^{-1} at 80 °C), and reduced methanol permeability (*i.e.*, 3.91·10^{-8} cm^2·s^{-1}) upon increasing the number of coating layers on the S-NWF, (c) achievement of a membrane selectivity value of 2.61·10^6 S·s·cm^{-3}, and (d) the fact that 6 layers of coating resulted in producing the highest peak power density of 62.32 W·m^{-2} and a current density of 540 A·m^{-2}.

Keywords: *polymer membranes, direct methanol fuel cell, proton exchange membrane, composite membrane electrolyte, poly(vinyl alcohol-co-styrenesulfonic acid)*

1. Introduction

In general, sulfonated polymer-based proton exchange membranes (PEMs) need a higher degree of sulfonation to attain adequate proton conductivity. This subsequently leads to the demonstration of high uptake of water and membrane swelling. This, in turn, results in dimensional instability and reactant (*i.e.*, methanol for direct methanol fuel cell; DMFC), crossover. Hence, physico-chemically modified sulfonated polymers are usually utilized to form composite membranes. With the aim of achieving thin and high-strength membranes, which can be stable under fuel cell operating conditions as well as provide minimal proton transport resistance, reinforced PEMs have been developed [1]. Composite PEMs can be prepared by adding inorganic [3–7] or organic

[8–13] fillers to the polyelectrolyte or by impregnating the polyelectrolyte into a mechanically stable and suitable microporous polymer support [14–16]. In this direction, researchers have made several attempts to fabricate reinforced composite membranes. For example, Penner and Martin [2] impregnated polytetrafluoroethylene (PTFE) based porous support with perfluorosulfonic acid (PFSA) to develop a thin cation exchange membrane [2]. Also, in the past, DuPont had developed PTFE-reinforced composite membranes, known as Nafion® 324 and 417 [1]. Further, to reduce the proton transport resistance, the microporous expanded PTFE support membranes have been impregnated with PFSA [17–21]. Again, to reduce methanol permeation through the PEM for DMFC application, Chen *et al*. [22] have prepared Nafion-impregnated PTFE PEMs. Pandey *et al*. [23] have used porous polyvinylidene fluoride (PVDF) membrane, with impregnated ionic fillers, for the reduction of methanol crossover. Recently, Cheng *et al*. [24] have used polyimide nanofibrous mat as the reinforcing agent for the preparation of PEMs, using sulfonated poly(fluorenyl ether ketone) (PEEK) for DMFC applications. The resulting composite membrane showed a 65.8% higher mechanical strength than the PEM made from neat sulfonated PEEK. Similarly, non-woven fabric (NWF) can also be used as a support for the preparation of composite PEMs, as demonstrated by Thakur *et al*. [14] by employing polypropylene (PP)-based NWF. Additionally, in order to improve hydrophilicity, the PP-based NWF was modified by a plasma-assisted polydopamine coating. On the other hand, Vicente *et al*. [25] have used a sulfonation route to modify PP-based NWF, using sulfuric acid as a sulfonating agent. Employment of such surface modification techniques, using dopamine and sulfuric acid, resulted in an improvement in the hydrophilicity of the PP-based NWF.

This paper, for the first time, reports the fabrication of reinforced composite PEMs by using poly(vinyl alcohol-*co*-styrenesulfonic acid) (PVA-*co*-SSA) as the polymer electrolyte and NWF as the reinforcing agent. In essence, the use of low-cost porous NWF, having a thinner cross-section, as a reinforcing agent can help in producing PEMs with lower thickness and cost, along with moderate proton conductivity and mechanical strength. Accordingly, this study is based on the use of thin PP-based NWF for the preparation of composite PEMs, with the aim of examining

the applicability of functionalized, *i.e.*, sulfonated PP-NWF (S-NWF), as the reinforcing fabric to obtain dimensionally stable PEMs. Sulfonation of the PP-NWF was done in order to decrease the ionic resistivity and to impart polar groups ($-SO_3$) for better wettability with the polymer electrolytes. The use of S-NWF for reinforced composite membrane preparation was expected to produce thin membranes while maintaining mechanical integrity. Furthermore, this study also investigates the physicochemical properties of S-NWF, as well as the final composite PEMs. Lastly, various characteristic properties of the resultant PEMs and their performance in DMFC have been thoroughly examined.

2. Experimental
2.1. Materials
PP-NWF (10 g per square meter, thickness of 23 μm) was procured from Hirose Paper Mfg. Co. Ltd, Japan. The copolymer PVA-*co*-SSA ($\overline{M}_w$: 270 926 g/mol, *PDI*: 2.84) was synthesized in the authors' laboratory, as reported elsewhere [26]. The anode gas diffusion electrode (GDE) loaded with 0.5 mg·cm^{-2} of 60% platinum (Pt), the cathode GDE containing 0.5 mg·cm^{-2} of 60% platinum-ruthenium (Pt-Ru), gaskets (Teflon-coated fiberglass) having 0.22 and 0.1 mm thickness, and Nafion-117 membrane were purchased from Sai Energy Fuel Cell Pvt. Ltd., India. Hydrochloric acid (HCl) (35%, AR) was procured from HiMedia Laboratories Pvt. Ltd., India. Sulfuric acid (98%, AR) and sodium hydroxide (extra pure) were purchased from Sisco Research Laboratories Pvt. Ltd., India. A 25% aq. solution of glutaraldehyde (GA) (Grade-II), and methanol (LR grade) were obtained from Rankem, India.

2.2. Methodologies
2.2.1. Surface modification of PP-NWF
Chemical modifications of PP-NWF were performed using concentrated sulfuric acid to impart functional groups and to improve the hydrophilicity. For this purpose, the PP-NWF samples were immersed in concentrated sulfuric acid solution (98%) under continuous stirring at 90 °C. The modified specimens were removed from the reaction medium at different intervals of time to optimize the reaction time. The resulting acid-modified PP-NWF (S-NWF) was then kept under running deionized (DI) water until the complete removal of the adhered sulfuric acid.

2.2.2. Preparation of composite PEMs

10 g of PVA-*co*-SSA was dissolved in 100 ml DI water at 80 °C for 30 min to get a 10% (w/v) solution. To this solution, 5 wt% of GA was added, followed by adjustment of the pH of the dope solution to 2–3 by adding 2–3 drops of 0.5 N sulfuric acid solution under continuous stirring. The membrane fabrication was carried out by employing a dip-coating technique, wherein an S-NWF sample of 10 cm ×10 cm size was immersed into the dope solution, contained in a beaker, for about 3 min. Following this, the membrane sample was removed and was vertically suspended to drain the excess dope solution and was allowed to crosslink at room temperature until it became dried and solidified. This single-layered PEM was designated as C-PEM-1L. Further, to increase the thickness of the coating layer, this coating procedure was repeated two, three, and six times and the obtained membranes were designated as C-PEM-2L, C-PEM-3L, and C-PEM-6L, respectively. The membrane, prepared with 1, 2, 3 and 6 coating layers onto the S-NWF, was first dried at 25 °C for 24 h, and then finally heat-treated in a hot air oven at 45 °C for 12 h. A representation of the composite membrane preparation has been shown in Figure 1.

2.2.3. Characterization of PP NWF and composites PEMs

S-NWF and composite PEMs based on PVA-*co*-SSA/ S-NWF were characterized using Fourier transform infrared spectroscopy (FTIR) (Nicolet-6700, Smart Orbit, USA), in attenuated total reflection (ATR) mode, within the scanning range of 500–4000 cm^{-1}. Thermogravimetric analysis (TGA-Q50, TA Instruments, USA) of the membranes was performed with a heating rate of 10 °C·min^{-1} under an inert nitrogen atmosphere. X-ray diffraction (XRD) (XRD-7000, Shimadzu, Japan) analyses of the membranes were done at a 2θ range of 5–80°. The surface topographies of PP-NWF and S-NWF were studied by scanning electron microscopy (SEM) (EVO MA 15, Carl Zeiss SMT, Germany) after gold/palladium sputter

coating in IEC34 – a DC plasma sputter coating instrument. Morphologies of the composite PEMs were examined by field-emission gun scanning electron microscope (FEG-SEM) (Geminisem300-Zeiss, Germany). For the cross-sectional surface examination, the PEM samples were fractured after freezing in liquid nitrogen. Before FEG-SEM characterization, gold-palladium coating was applied to the membrane specimens by using a sputter coater (SC7620) to minimize the charging effect. Tensile properties of the membrane specimens were determined by a universal testing machine (UTM) (Instron 3382A, UK). For testing, the membrane samples of 10 cm×2 cm size each were fixed between the grips of UTM and tested at a crosshead speed of 10 mm·min^{-1}, using a 1 kN load cell. The resulting stress-strain curves were recorded automatically using Blue Hill. A minimum of three samples were tested under the same condition, and the average results have been reported. The modulus of toughness values of NWF and composite membranes were determined by the calculating area under the stress-strain curve up to the fracture point as described in [27]. The static contact angles of the membrane surfaces were determined using contact angle goniometer (APEX Instrument, DataPhysics, Germany) by employing distilled water droplet as a contacting liquid onto the sample surface that was fixed to the flat glass surface by double-sided tape.

Degree of sulfonation, water uptake, and swelling studies

The degree of sulfonation of PP-NWF was measured by first taking the dry weight of the neat PP-NWF and S-NWF. The degree of –SO$_3$ group substitution in acid-modified NWF (S-NWF) is reported in weight %. Degree of sulfonation (mol%) for the optimized sample (*i.e.*, S-NWF, acid treatment given for 21 h) was calculated using TGA data according to methods reported elsewhere [28]; wherein the polymer's (*i.e.*, PP) repeating unit weight (44 g·mol^{-1}), and –SO$_3$'s weight (80 g·mol^{-1}) were taken into consideration
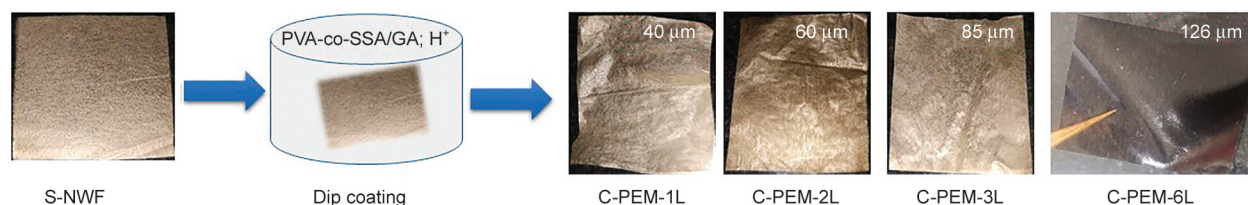

Figure 1. A schematic presentation of the fabrication of PVA-*co*-SSA/S-NWF composite PEMs, along with the photographs of the prepared membranes.

for the calculation of equivalent weight. While for water-uptake measurement of S-NWF and PEMs, at first, the weights of the dried membrane samples (W_{DM}) were measured. Then, water uptakes of the S-NWF/PVA-*co*-SSA-based composite membranes were evaluated by dipping the membrane samples into distilled water for 24 h at temperatures of 25, 60, 70, and 80 °C. Following this, the swollen membranes were taken out and wiped with tissue paper, and the weights of the wet membranes were recorded (W_{WM}). Finally, the water-uptake values were determined by employing Equation (1):

Water-uptake by membrane [%] =

$$= \frac{W_{WM} - W_{DM}}{W_{DM}} \cdot 100 \qquad (1)$$

To study membrane swelling in water, the dried membranes of a known thickness (T_{DM}) and dimension, *i.e.*, area (A_{DM}) of 7 cm×7 cm, were kept immersed in water (under different temperatures of 25, 60, 70, and 80 °C). After 24 h, the swollen membranes were removed from the water and were wiped dry with Kimwipe. Following this, the thicknesses of the water-swollen membranes (T_{SM}) were measured, and finally, the % swelling thickness of the membranes was computed using Equation (2). For the measurement of the % swelling of the membranes by area, the change in membrane area after water swelling (A_{SM}) was first measured, followed by the determination of the % area swelling by employing Equation (3):

Membrane swelling by thickness [%] =

$$= \frac{T_{SM} - T_{DM}}{T_{DM}} \cdot 100 \qquad (2)$$

Membrane swelling by area [%] =

$$= \frac{A_{SM} - A_{DM}}{A_{DM}} \cdot 100 \qquad (3)$$

Ion exchange capacity (IEC)
For this purpose, the membrane specimens were first kept in solutions of 1 M HCl for 1 h, and then washed with DI water. The membranes were then dipped in 1 M aqueous solution of NaCl for 1 h for conversion to Na⁺ form and were subsequently rinsed with DI water. This regenerating procedure of PEMs was repeated three times. Finally, the PEMs in the H⁺ form

were immersed in 0.1 M NaCl solutions for 24 h, and the liberated HCl for each membrane was quantitatively estimated by titration against 0.1 M aqueous solution of NaOH. The *IEC* was determined by utilizing Equation (4) [29]:

$$IEC \left[meq \cdot g^{-1} \right] = \frac{V_{NaOH} \cdot N_{NaOH}}{W_{DM}} \cdot 100 \qquad (4)$$

where V_{NaOH} denotes the volume of NaOH consumed during the titration [ml], N_{NaOH} represents the normality of NaOH solution, and W_{DM} indicates the dry membrane weight in [g].

Proton conductivity measurement
For determining the proton conductivity, PEM samples were initially activated by keeping them in 0.1 N HCl for 1 h. The conductivities of the fully hydrated PEMs were analyzed using the four-probe electrochemical impedance spectroscopy (EIS) (PARSTAT MC-1000, USA) method by scanning the samples over an AC frequency range of 1 Hz to 1 MHz at a voltage magnitude of 50 mV. The proton conductivity values of PEMs were evaluated by employing Equation (5) [30]:

$$\sigma_{PEN} \left[S \cdot cm^{-1} \right] = \frac{1}{R_{PEM}} \cdot \frac{l_{electrodes}}{W_{PEM} \cdot T_{PEM}} \qquad (5)$$

where, σ_{PEM} is the conductivity of protons [S·cm⁻¹], while l electrode, R_{PEM}, W_{PEM} and T_{PEM} denote the distance between the electrodes [cm], measured impedance of the PEM [Ω], width of the membrane [cm], and specimen thickness [cm], respectively.

Measurement of methanol permeability and selectivity
Methanol permeability (P_{PEM}) of the membrane specimens was determined in a diffusion cell consisting of two glass compartments [31]. For this purpose, a PEM test sample was placed in between two compartments, along with appropriate gaskets, to form a two-compartment cell, and the system was clamped to make it leakproof. One compartment A contained a 2 M solution of methanol, while the other compartment B was filled with DI water. The solutions in the two compartments were constantly stirred at 25 °C, while methanol from the feed solution slowly permeated from compartment A to the permeate compartment B. After 12 h, the sample solutions from the feed and the permeate compartments were collected, and the content of methanol in water

was analyzed by gas chromatography mass spectroscopy (GCMS-QP2010, Shimadzu, Japan). The methanol permeability was calculated using Equation (6):

$$P_{PEM}\,[cm^2 \cdot s^{-1}] = \frac{T_{PEM} \cdot V_B}{A_{PEM} \cdot t} \cdot \ln\left(\frac{C_B^0 - C_A}{C_B^t - C_A}\right) \qquad (6)$$

where P_{PEM} denotes the methanol permeability [$cm^2 \cdot s^{-1}$] of PEM, T_{PEM} is the membrane thickness [cm], V_B is the solution volume in the compartment B [cm^3], A_{PEM} is the active area of PEM [cm^2], C_B^0 and C_B^t is the concentration of methanol [$mol \cdot l^{-1}$] in the compartment B at the starting of experiment (*i.e.*, at $t = 0$) and after time t [s] respectively. C_A represents methanol concentration in compartment A.

The membrane selectivity was calculated by dividing the obtained proton conductivity (σ_{PEM}) by methanol permeability (P_{PEM}), using Equation (7):

$$PEM\ selectivity\ [S \cdot cm^{-3}] = \frac{\sigma_{PEM}}{P_{PEM}} \qquad (7)$$

The performance of the DMFC, assembled with a single cell and fed with methanol as the fuel, was evaluated using a DMFC station (WonATech, South Korea). For this purpose, a composite PEM was placed between the cathode and the anode GDEs. To decrease the interfacial distance between the layer of catalyst and the surface of the membrane, this sandwich structure was pressed at a temperature of 60 °C using a compression press (HP 80 T, Neoplast Engineering Pvt. Ltd., India) under a minimum platen holding pressure for 2 min. The polarization curve, *i.e.*, current-voltage (*i–V*), was obtained by running the fuel cell at 60 °C under a constant supply of 2 M solution of methanol feed at a flow rate of 2–10 ml·min^{-1} at the anode side; while O$_2$ gas was supplied to the cathode side at a flow rate of 200 cm^3·min^{-1}. All the membranes (in membrane-electrode-assemblies, MEAs) were tested in the fuel cell working station, and the *i–V* characteristics curves were automatically reported via the FCT server. Similar conditions were maintained for the testing of all the MEAs.

3. Results and discussion
3.1. Optimization of the surface modification of PP-NWF

As the reaction time increased from 3 to 30 h, the extent of grafting, water-uptake, and *IEC* of the S-NWF was found to get increased from 1.12 to 43%, 4.95 to 56% and 0.026 to 0.38 meq·g^{-1}, respectively (Figure 2). Although the physicochemical
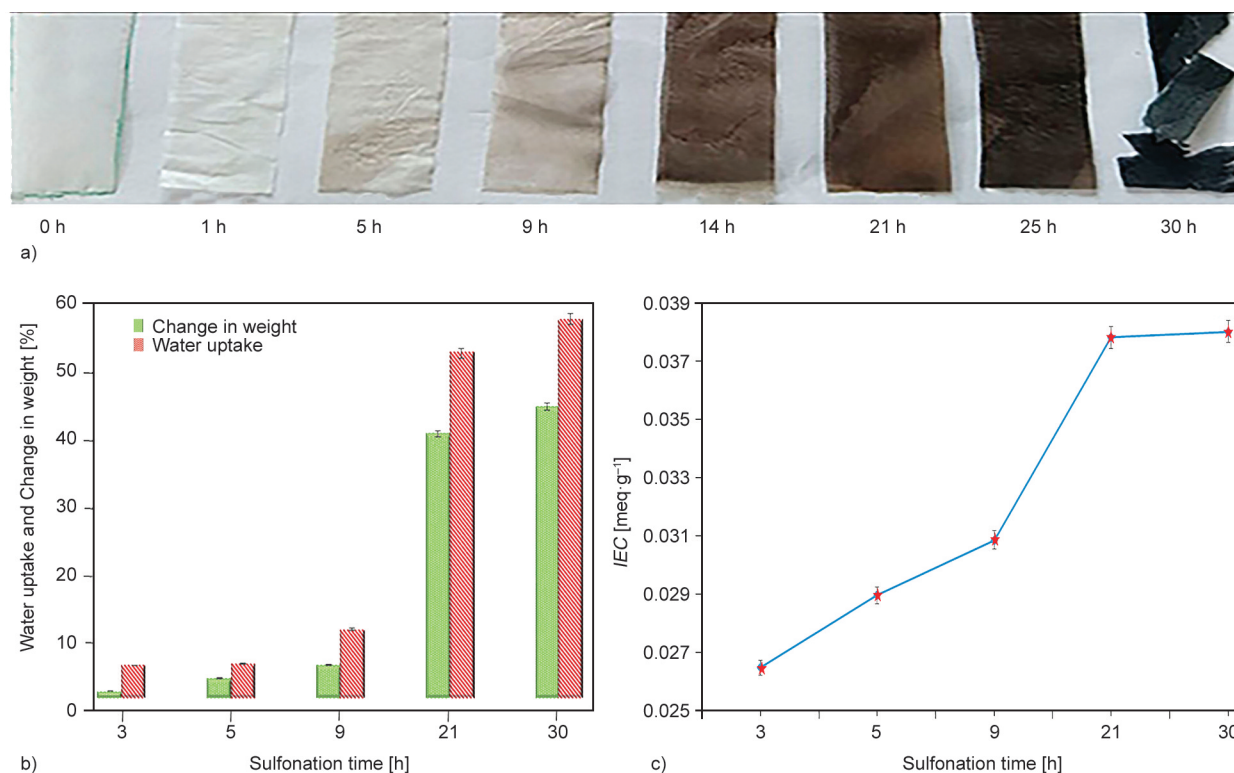

Figure 2. (a) Photograph of the PP-NWF and S-NWFs taken after different sulfonation intervals, (b) change in weight of PP-NWF after sulfonation, and water-uptake [%], and (c) *IEC* for sulfuric acid modified S-NWF with respect to the reaction time.

properties of the PP-NWF were found to increase at higher sulfonation times, a reaction duration of more than 21 h resulted in a reduction in the tensile strength
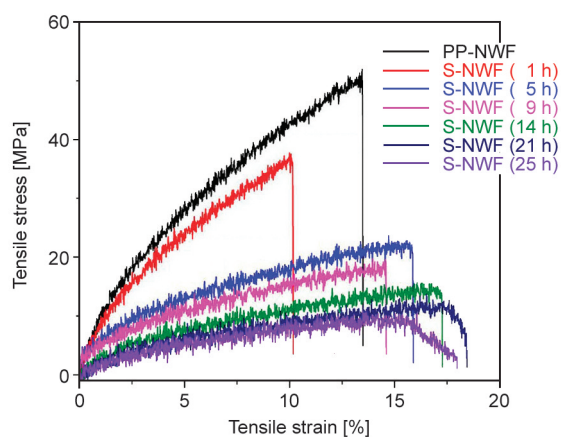

Figure 3. Engineering stress-strain curves obtained from tensile tests of the neat (PP-NWF) and sulfonated (S-NWF) sulfonated at different times.

Table 1. Tensile properties of neat and sulfonated PP-NWFs.

PP-NWF and S-NWFs	Tensile strength [MPa]	Modulus of toughness [MPa]
PP-NWF	52.0±4.4	4.2±0.7
S-NWF-1 h	37.8±1.0	2.3±0.5
S-NWF-5 h	23.6±0.6	2.4±1.2
S-NWF-9 h	19.7±0.5	1.8±1.0
S-NWF-14 h	16.3±1.5	1.6±0.2
S-NWF-21 h	13.3±0.5	1.4±0.1
S-NWF-25 h	10.8±1.2	1.4±0.6

and an enhancement in the brittleness of the PP-NWF (Figure 3 and Table 1) without much improvement in the *IEC* values (Figure 2c). Hence, the sulfonation of PP-NWF was performed by dipping in sulfuric acid for 21 h, which was considered for further preparation of the composite PEMs. The optimized properties of the neat (PP-NWF) and the modified (S-NWF) NWF have been shown in Table 2.

Modifications induced by sulfuric acid treatment on PP-NWF were established by FTIR. The spectra of the neat PP-NWF and modified S-NWF have been presented in Figure 4. The neat PP-NWF showed characteristic peaks of PP at 2914, 2847, 1461, 1375, and 718 cm^{-1} [32, 33]. The prominent peaks at 2914 and 2847 cm^{-1} can be attributed to the stretching vibration of –CH and –CH$_2$, while bands at 1461 and 1471 cm^{-1} are due to the bending vibrations from –CH and –CH$_2$ groups of polyolefins. The rocking vibration of CH is clearly noticeable at 738 cm^{-1} [32]. It is well known that sulfonation of PP solid surface using hot concentrated sulfuric acid takes place through electrophilic addition reaction of –SO$_3$ [34]. Also, it has been proved that the pedant CH$_3$ groups of PP are more likely to experience sulfonation than the C atoms of the backbone chain, forming the major product. On the other hand, minor product (*i.e.*, alkene sulfonic acids) is also expected to get produced due to the formation of unstable β-sultone and subsequent breaking of the β-sultone ring-structure

Table 2. Water-uptake, *IEC*, surface wettability, and mechanical properties of unmodified PP-NWF and modified S-NWF (sulfonation for 21 h at 90 °C).

Membranes	Grafting [%]	Water-uptake [%]	*IEC* [meq·g^{-1}]	Water contact angle [°]	Tensile strength [MPa]
PP-NWF	–	–	–	107.23	52.0
S-NWF	39.0[a] 16.9[b]	50.92	0.0378	77.32	13.3

[a]degree of sulfonation in weight %
[b]degree of sulfonation [mol%] calculated using TGA data according to methods described in [28]; wherein polymer (*i.e.* PP) repeating unit weight (44 g·mol^{-1}), and –SO$_3$ weight (80 g·mol^{-1}) were taken into consideration for calculation of equivalent weight.
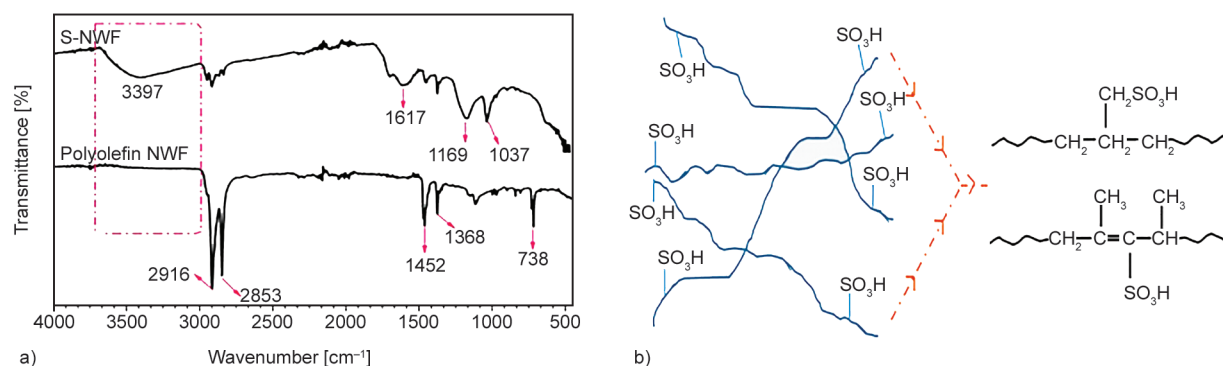

Figure 4. (a) FTIR spectra of the neat PP-NWF and modified S-NWF, and (b) proposed chemical structure of S-NWF.

[35]. For example, the band at 738 cm^{-1} that appeared due to –C–H bending of the –CH$_3$ pedant groups of PP in PP-NWF got disappeared after sulfonation, which indicates that the sulfonation has predominantly occurred via electrophilic addition reaction at the –CH$_3$ pedant groups of PP-NWF. Additionally, a new broad peak that appeared at 1700–1660 cm^{-1} was due to the formation of C=C bonds and breaking of the β-sultone ring-structure, owing to the addition of –SO$_3$ group at the 3° carbon atoms of PP. Accordingly, the expected structure of S-NWF is shown in Figure 4b. After sulfonation of PP-NWF, the appearance of new peaks at 3397, 1617, 1169, and 1037 cm^{-1} are clearly visible in the FTIR spectra of S-NWF, which indicates successful sulfonation [25]. The broad band in between 3000 to 3500 cm^{-1} shows the existence of hydrophilic –SO$_3$H groups that have been chemically bonded to PP during the sulfonation reaction. While other broad bands at 1169 and 1037 cm^{-1} appeared due to the asymmetric stretching modes of –S=O [36]. The intensity of asymmetric and symmetric stretching vibrations of –CH$_2$ and –CH groups (appearing at 2924 and 2862 cm^{-1}, respectively) of PP-NWF was found to sharply decrease after sulfonation (*i.e.*, for S-NWF).

The evolution of the surface morphology of the neat and modified S-NWF by SEM (Figure 5) revealed that after the sulfuric acid treatment, the surface of the NWF became rougher. This may be due to the surface etching of PP fibers by sulfuric acid. However, no major chemical degradation and breaking of the fibers were observed. Although slight swelling of the fibers took place, the porous structure of the PP-NWF and S-NWF seems almost similar. It is to be noted here that since sulfuric acid-induced chemical modification occurred on the surface of the fibers, the solvation of the fibers by sulfuric acid was only limited to the outer surface of the fibers. Therefore, no apparent visible changes were observed in S-NWF. It is believed that the presence of polar ionic groups (–SO$_3$H) imparted partial hydrophilicity in S-NWF, hence it can act as a suitable reinforcing fabric for the preparation of PEMs having lower methanol permeability.

3.2. Functional groups analysis of the composite membranes by FTIR

Anchoring of the –SO$_3$H functional groups onto the microfibers of PP-NWF via acid treatment resulted in an increase in *IEC* and hydrophilicity. Further, before applying the coating of PVA-*co*-SSA dope solution, an acid-treated PP-NWF was subjected to chromic acid treatment to improve the interfacial adhesion between PVA-*co*-SSA and PP microfibers. Impregnation of S-NWF fabric with polymer dope solution resulted in the formation of a uniform layer onto the fibers and produced thin PEMs. During the impregnation of S-NWF with PVA-*co*-SSA, GA was mixed to the polymer solution to induce crosslinking. The chemical structures of the PEMs prepared by applying different coating layers were analyzed by FTIR, and the resulting spectra of the membranes have been presented in Figure 6. The presence of a wide peak between 3600 to 3000 cm^{-1} was attributed to intra- and inter-molecular H-bonds among the hydroxyl (–OH) groups attached to the copolymer chain and the –SO$_3$H groups present in both the copolymer and the modified S-NWF. The small intense peaks at 2924 and 2862 cm^{-1} were related to
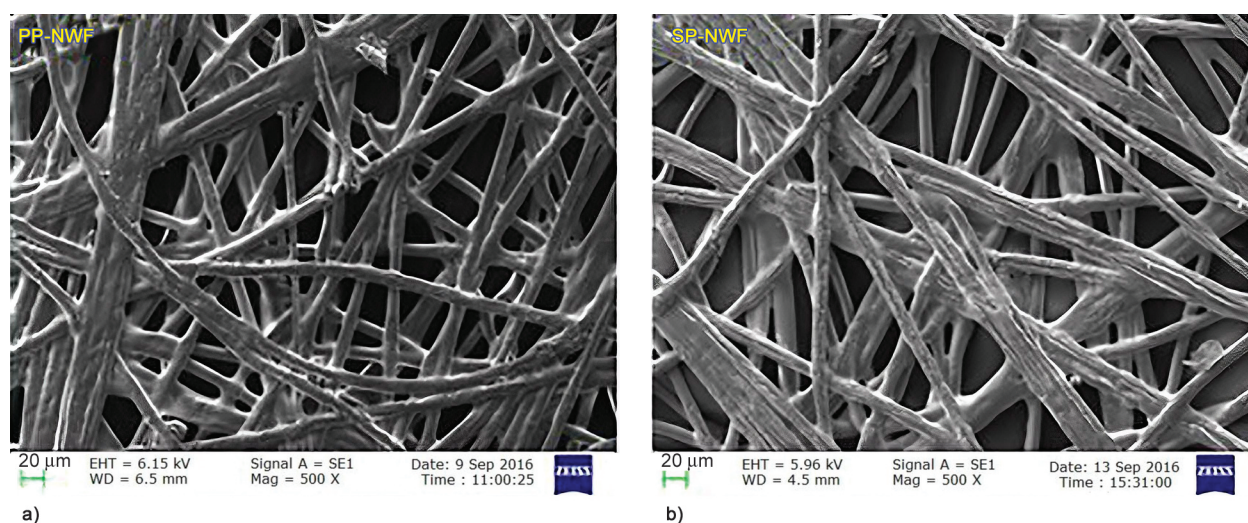

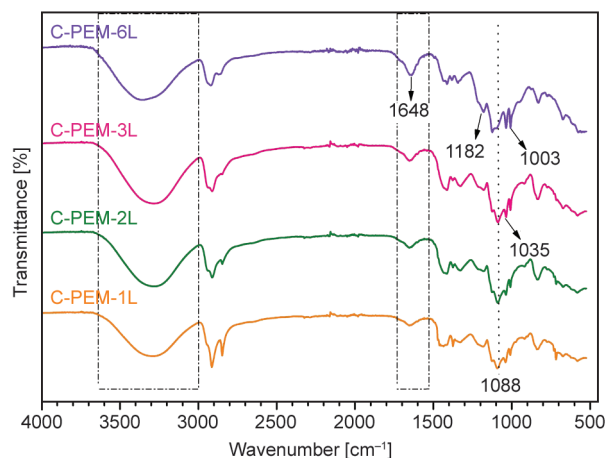**Figure 5.** SEM micrographs of (a) neat PP-NWF, and (b) modified S-NWF membranes.

Figure 6. FTIR spectra of composites membranes: C-PEM-1L, C-PEM-2L, C-PEM-3L and C-PEM-6L.

the asymmetric and symmetric stretching vibrations of –CH$_2$ group, while the band appearing at around 1653 cm^{-1} was due to the aromatic ring (present in PVA-*co*-SSA) mode that involves C–C stretching as well as C–C contracting. The presence of –SO$_3$H groups in the copolymer repeating unit was also confirmed by the appearance of asymmetric stretching vibrations of O=S=O at 1182 and 1003 cm^{-1}. The characteristic stretching vibrations at 1411 cm^{-1} revealed the partial crystallinity of the copolymer chain [26]. A new carbonyl (–C=O) peak at 1709 cm^{-1} that appeared was probably due to the anchoring of one end of GA to the copolymer, while the other end remained unreacted. Most importantly, the crosslinking of PVA-*co*-SSA by GA was confirmed by the presence of the peak at 1092 cm^{-1} due to acetal (–C–O–C) formation [37, 38]. Overall, the intensities of the characteristic peaks assigned to the neat PP-NWF, *i.e.*, 2924 and 2862 cm^{-1} for asymmetric and symmetric

stretching vibrations of –CH$_2$ and –CH group, respectively, gradually reduced after subsequent coating layers of PVA-*co*-SSA/GA solution; and a peak between 1182 and 1003 cm^{-1} (that appeared due to asymmetric stretching vibrations of O=S=O in S-NWF) became broader with an increasing number of PVA-*co*-SSA/GA coating layers. This observation indicates that the PVA-*co*-SSA/GA coating is uniform, and it completely covers the underlying chemically modified S-NWF support when impregnated in the polymer solution.

3.3. Water-uptake, swelling, and hydrophilicity of the membranes

Water uptake is a very crucial property of PEM. This is because in DFMC, the conduction of protons through the membrane takes place via H-bonding of hydronium ions with the anchored ionic groups as well as the presence of water molecules within the PEM matrix. High water uptake facilitates proton transport; however, water uptake also affects the dimensional stability of the PEM. Hence, a balance between water uptake, membrane swelling, and proton conductivity is required to obtain an optimized DMFC performance. Figure 7a presents the % water-uptake of the composite membranes evaluated by immersing the membrane specimens in distilled water at different temperatures, followed by analyzing the weight gain of the samples. It can be seen that an enhancement in the weight of the PEMs (by increasing the layer of coating) resulted in a slow enhancement of the water uptake, which can be due to the increasing availability of water affinity sites within a unit area of the membrane. For instance, as coating layer
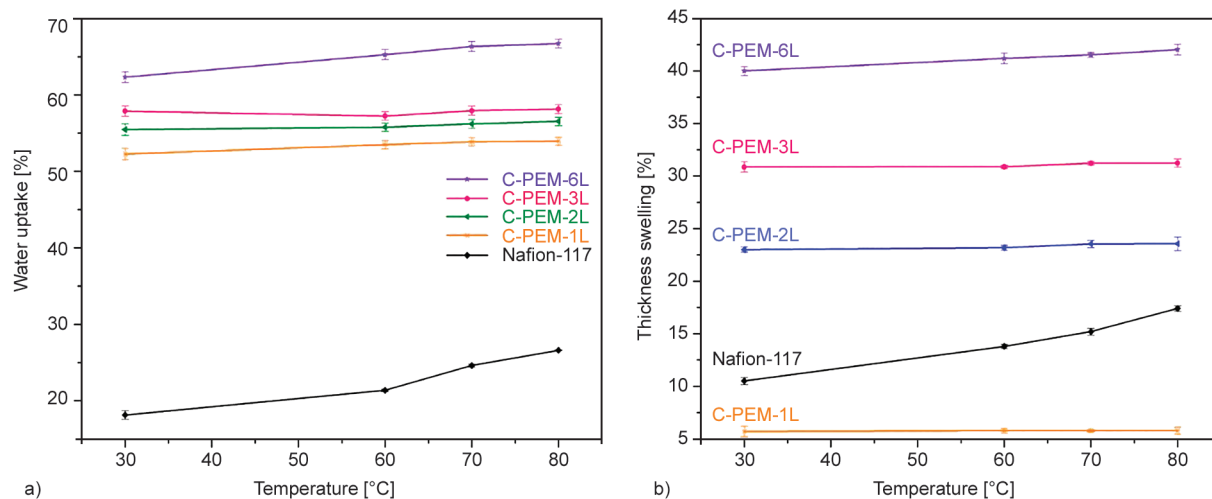

Figure 7. (a) Water uptake [%], and (b) swelling by thickness [%] of composite PEMs and Nafion membrane immersed into distilled water at different temperatures.

increased from one (C-PEM-1L) to six (C-PEM-6L), the % water-uptake got increased from about 52 to 62% at room temperature. However, upon increasing the water temperature to 80 °C, there was little effect on the water absorption capacity of the membranes. This observation indicated that all the membranes were crosslinked, and immersion of such membranes in hot water did not prominently increase the polymer chain relaxation. Moreover, all the composite membranes exhibited higher water uptake than Nafion-117, *i.e.*, values of 18.19 and 26.64% at 25 and 80 °C, respectively. Therefore, this result is promising for the application of PVA-*co*-SSA/S-NWF-based composite membranes in DMFC at 60 to 80 °C. Upon immersion of the membranes in water at varying temperatures, the obtained variation of the thickness of the swelled membranes is shown in Figure 7b. It can be clearly observed that an increase in the membrane thickness with the increment in the number of applied coatings on S-NWF induced a gradual increment in the swollen thickness of the membranes when immersed in water. Swelling in thickness directly depends on the dry thickness of the membranes as well as the temperature of the swelling medium, *i.e.*, water. In this study, it was realized that the dry thickness factor more prominently affected the membrane swelling than water temperature. The thickness swelling of the composite membranes was observed in the order of 5.772% (C-PEM-1L) < 23.56% (C-PEM-2L) < 31.225% (C-PEM-3L) < 42.03% (C-PEM-3L), when the membranes were immersed in water having a temperature of 25 °C. In the case of Nafion-117, about 10 and 17% swelling of thickness were observed in water having a temperature of 25 and 80 °C, respectively. On the other hand, there were no apparent changes in the area of composite membranes when they were dipped in water at 25 or 80 °C, which was due to the reinforcement effect between S-NWF and PVA-*co*-SSA. Thus, the use of chemically modified S-NWF for composite

membrane preparation showed appreciable water uptake without prominent change in the membrane area and thickness in water even at 80 °C.

The surface hydrophilicity of the membranes, evaluated by using a water droplet as a wetting liquid, is given in Figure 8. As anticipated, with an increase in layer count of coating onto the S-NWF, the hydrophilicity of the membranes got enhanced. This was because of the increasing water uptake of the membranes and the availability of more functional groups on the membrane surface that facilitated water interaction through H-bonding.

3.4. Thermo-mechanical characteristics of the membranes

Thermogravimetric investigation of the S-NWF and the composite PEMs were performed under an inert atmosphere between 25 and 800 °C, with a heating rate of 10 °C·min^{-1}. The % change in the weight of the membrane samples with respect to temperature is displayed in Figure 9.
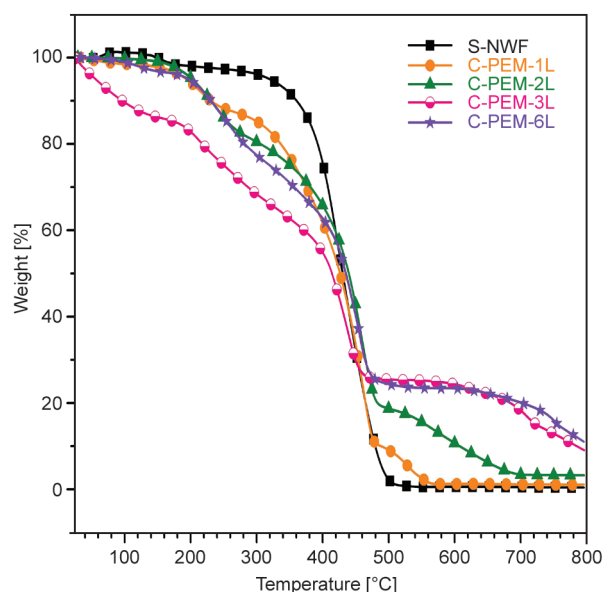

Figure 9. TGA analysis of S-NWF, C-PEM-1L, C-PEM-2L, C-PEM-3L, and C-PEM-6L.
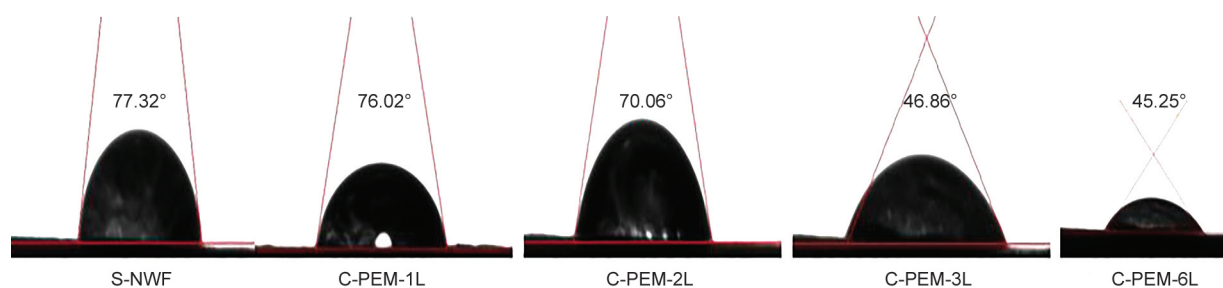

Figure 8. Water contact angle of S-NWF, and composite membranes (C-PEM-1L, C-PEM-2L, C-PEM-3L and C-PEM-6L).

The weight losses in the different temperature zones are usually associated with physical events due to second-order phase transitions like evaporation and desorption and chemical phenomena like degradation and dehydration in the membrane samples. In general, one of the most used criteria to evaluate the thermal stability of a polymer is the temperature at which 3% of its total weight is lost, while the residual percentage can be attributed to different factors. However, in the case of the present study, the polymer that has been used for PEM preparation is hygroscopic in nature. Hence, this generalized rule cannot be strictly applied to this polymer. Here, the initial loss in weight between 5 to 10%, in the temperature regime of 25–150 °C, was expected due to the removal of water molecules from the samples. Upon increase in temperature from 200 to 350 °C, the composite PEMs showed gradual weight loss. This is believed to be due to the removal of thermally labile functional groups, such as $-SO_3H$ and $-OH$, that was anchored to the polymer chains. The final loss of weight observed in the temperature regime of 350 to 500 °C can be ascribed to thermal degradation of the main chain of the polymer. The residual weight obtained at a temperature beyond 500 °C was higher for the composite membranes than the S-NWF, which may be due to the crosslinked structure of PVA-*co*-SSA.

The strength of the reinforced composite PEMs was measured at room temperature (25 °C) using a UTM. The engineering stress-strain curve obtained for the PEMs is presented in Figure 10. It was observed that the graphs moved monotonically downward as the number of coating layers increased; correspondingly, the tensile modulus and the tensile strength got reduced with a decrease in the thickness of the composite membranes. As expected, the elongation at break got reduced with increasing membrane thickness. The observed stress-strain characteristics indicated that more or less the membranes are isotropic since the use of S-NWF provides uniformity in all directions. Thus, an increase in the crosslink sites with an increasing coating layer resulted in higher mechanical strength of the prepared composites membranes, which is beneficial for fuel cell applications.

3.5. *IEC* and proton conductivity of the membranes

IEC and proton conductivity of PEMs are very vital parameters, as the proton transport through the membrane relies on the number of ionic sites available and water-uptake capacity [39]. *IEC* denotes the total number of ion-exchange groups available in the PEMs. Values of *IEC* in milliequivalent per gram [meq·g⁻¹] of the dry PEM, determined by the acid-base titration method, have been presented in Figure 11. As observed from the figure, the values of the *IEC* for C-PEM-2L, C-PEM-3L, and C-PEM-6L get improved with the increasing number of coating layers. This is due to the increase in the fraction of the polyelectrolyte in the composite PEM, leading to an increase in equivalent weight with respect to
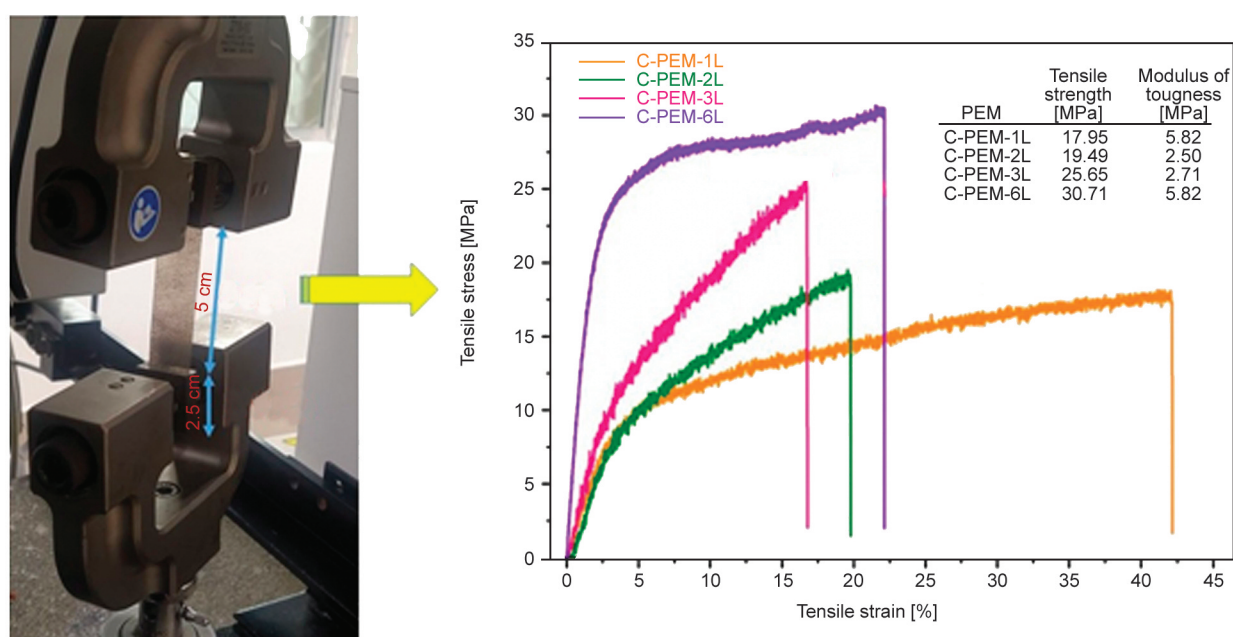

Figure 10. Engineering stress-strain curves were obtained from tensile tests of the composite PEMs at 25 °C.
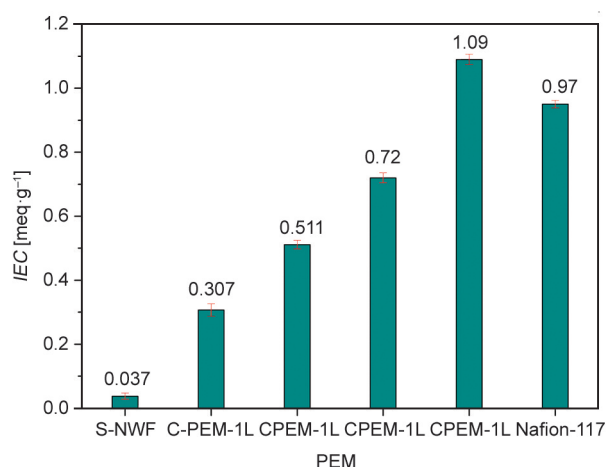
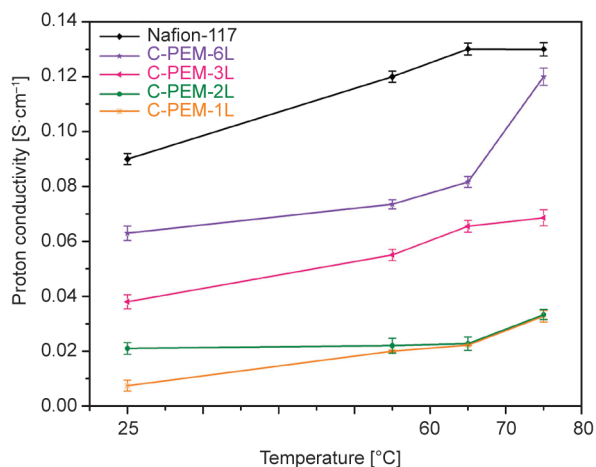**Figure 11.** *IEC* values of composites (C-PEM-1L, C-PEM-2L, C-PEM-3L and C-PEM-6L) and Nafion-117 membranes.

Figure 13. Proton conductivity values for the composited PEMs based on PVA-*co*-SSA at different temperature conditions.

ionic groups, such as –SO$_3$H and –OH. For example, C-PEM-6L produced an *IEC* of 1.09 meq·g^{-1} (which is quite similar to Nafion-117 which exhibited *IEC* of 0.97 meq·g^{-1}), while C-PEM-1L showed a much lower *IEC* of 0.307 meq·g^{-1}. The increase in the *IEC* of the PEMs with the number of coating layers applied is well in accordance with the observed increase in the water uptake by the membranes.

Similar to *IEC*, the proton conductivity of a PEM is directly associated with the performance of a fuel cell that consists of that PEM. The proton-conducting ability of the PEMs, tested in four probes EIS (Figure 12), is shown in Figure 13. Proton transport

through composite PEMs, based on PVA-*co*-SSA, is expected to occur by Vehicle and Grotthuss mechanisms (Figure 12) [40]. Increasing the thickness of the coating layer resulted in an enhancement in the *IEC* and the water uptake of the composite PEMs. Hence, the increased hydration behavior of the PEMs facilitated the proton transport along with water molecules (in the form of hydronium ions) by the vehicle mechanism. In addition, the exchange of protons via the formation of H-bond with ion-exchange sites, governed by the Grotthuss mechanism, facilitated proton migration. Due to this, as the number of the coating layer of the PEMs increased, an enhancement in the
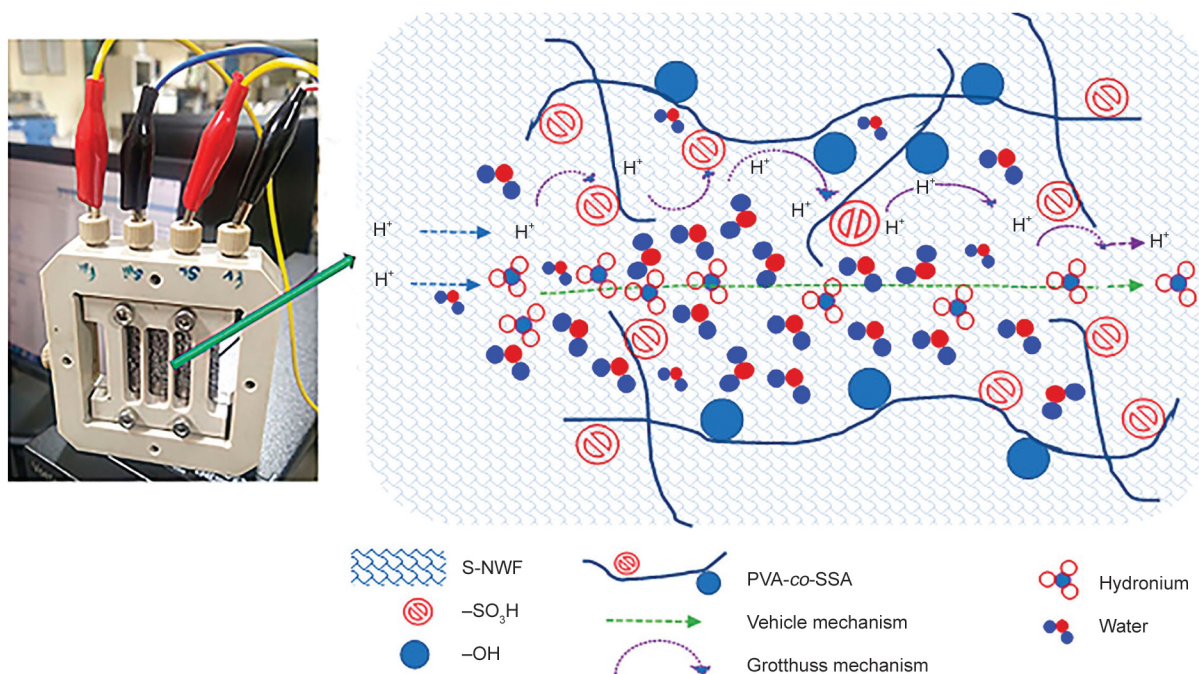

Figure 12. A four-probe cell used for proton conductivity measurement by EIS and the proposed proton transport mechanism in PVA-*co*-SSA-based composite PEMs.

proton conductivity was obtained. Furthermore, a rise in the temperature facilitated the migration of protons due to increased swelling and water uptake by the PEMs [41]. In this study, C-PEM-6L showed the highest proton conductivity values of 0.073, 0.081, and 0.12 S·cm^{-1} at 60, 70, and 80 °C, respectively. On the other hand, the proton conductivity values obtained for C-PEM-1L, C-PEM-2L, C-PEM-3L, and C-PEM-6L were 0.019, 0.02, 0,06, and 0.07 S·cm^{-1}, respectively, at 60 °C.

3.6. Methanol permeability and membrane selectivity of the PEMs

During the application of PEMs in DMFCs, the crossover (*i.e.*, permeation) of the fuel methanol from the anode to the cathode decreases the fuel utilization efficiency of the DMFC. Therefore, it is needed to fabricate PEMs having a higher proton-conducting ability and low methanol permeability. Low methanol permeation through a PEM from the anode compartment to the cathode compartment not only improves the performance of the DMFC but also prevents poisoning of the catalyst at the cathode side. The ratio of proton conductivity to methanol permeability is represented by the PEM selectivity [42]. Table 3 presents the methanol permeation as well as the PEM selectivity measured for the composite PEMs. It can be observed that all the membranes allowed very low methanol permeation in between $2.85 \cdot 10^{-7}$ and $3.91 \cdot 10$-8 cm^2·s^{-1}, as compared to Nafion-117 ($2.89 \cdot 10^{-6}$ cm^2·s^{-1}). It was further seen that the methanol permeation got reduced with an increasing number of the coating layer, in spite of increasing proton conductivity and water uptake of the PEMs. Methanol crossover through a PEM occurs due to diffusion, and hydrated hydronium ions and ionic sites attached to the membrane act as carriers. A reduction in the affinity of the PEMs for methanol molecules compared to molecules of water is expected due to the presence of PVA units in the PEMs.

Table 3. Methanol permeability and PEM selectivity of C-PEM-1L, C-PEM-2L, C-PEM-3L, and C-PEM-6L.

Membranes	Methanol permeability [cm^2·s^{-1}]	Membrane selectivity [S·s·cm^{-3}]
Nafion-117	$2.89 \cdot 10^{-6}$	$1.94 \cdot 10^4$
C-PEM-1L	$2.85 \cdot 10^{-7}$	$2.61 \cdot 10^4$
C-PEM-2L	$8.51 \cdot 10^{-8}$	$2.61 \cdot 10^5$
C-PEM-3L	$8.06 \cdot 10^{-8}$	$2.61 \cdot 10^5$
C-PEM-6L	$3.91 \cdot 10^{-8}$	$2.61 \cdot 10^6$

This is owing to the fact that PVA has a high selectivity for water molecules than methanol. Typically, a fully hydrolyzed PVA completely excludes methanol from the polymer matrix, and methanol acts as a non-solvent for PVA [43].

Lower methanol permeability and higher proton conductivity are the key factors for the suitability of a PEM in DMFC application. From a practical point of view, membranes should possess high selectivity. It was gratifying to note that the selectivity values for the composite PEMs were obtained between $2.61 \cdot 10^6$ and $2.61 \cdot 10^4$ S·s·cm^{-3}, which were more than Nafion-117 ($1.94 \cdot 10^4$ S·s·cm^{-3}) measured at similar conditions. The composite PEMs based on GA-crosslinked PVA-*co*-SSA/S-NWF showed lower methanol permeability and higher selectivity, as well as comparable proton conductivity to Nafion-117.

3.7. XRD characteristics of the PEMs

Crystalline behavior of PVA-*co*-SSA/S-NWF composite PEMs was examined in a 2θ scanning range of 5–80°. Figure 14 illustrates the XRD results obtained for C-PEM-1L, C-PEM-1L, C-PEM-2L, C-PEM-3L, and C-PEM-6L. The PEMs produced five distinctive 2θ values at 13.89, 16.75, 18.35, 21.40, and 23.73°, which are typically considered for the α-form of PP at (110), (040), (130), (111) and (041) planes, respectively [44]. Upon increasing the number of coating layers, the intensity of these planes got reduced, which was due to the increase in the fraction of PVA-*co*-SSA as well as crosslinking sites
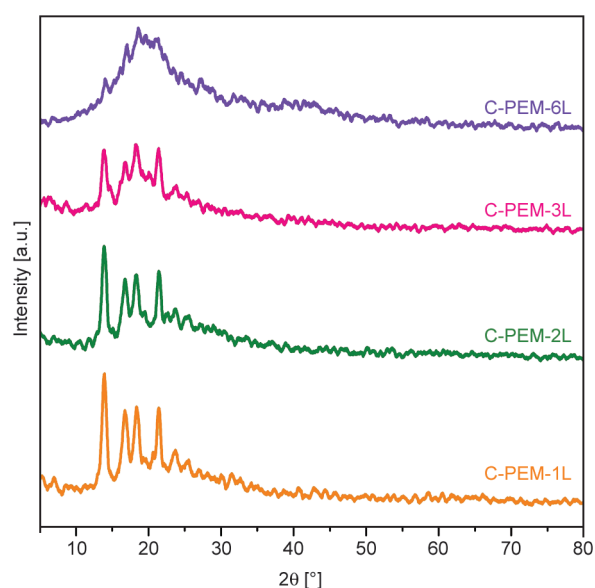

Figure 14. XRD graphs for PVA-*co*-SSA/S-NWF-based composite PEMs.

in the membranes. This got subsequently reflected in the decreasing crystallinity of the PEMs in the order of 66.9% (C-PEM-1L) > 59.49% (C-PEM-2L) > 56.63% (C-PEM-3L) > 48.54% (C-PEM-6L). Thus, the presence of both amorphous and crystalline regions in the PEMs caused enhancement in the proton conductivity values.

3.8. Morphology of PEMs

The surface morphology of the PVA-*co*-SSA/S-NWF-based membrane was examined by FEG-SEM after gold-palladium sputter coating. The obtained topography images of the composite PEMs are given in Figure 15. The micrographs revealed changes in the surface topography of S-NWF after impregnation with PVA-*co*-SSA/GA solution at different coating cycles, *i.e.*, number of layers of coating. The PEM coated with a single layer (C-PEM-1L) exhibited partially filled macropores of S-NWF. Further increase in the number of coatings resulted in the slow deposition of PVA-*co*-SSA onto S-NWF, and the membranes with 3 (C-PEM-3L) and 6 (C-PEM-6L) coating layers exhibited very plain surfaces with complete coverage of microfibers of S-NWF by the polyelectrolyte. Thus, the dip-coating technique adopted in this study was found to be very effective in controlling the coating layer thickness onto S-NWF for the fabrication of composite PEMs.
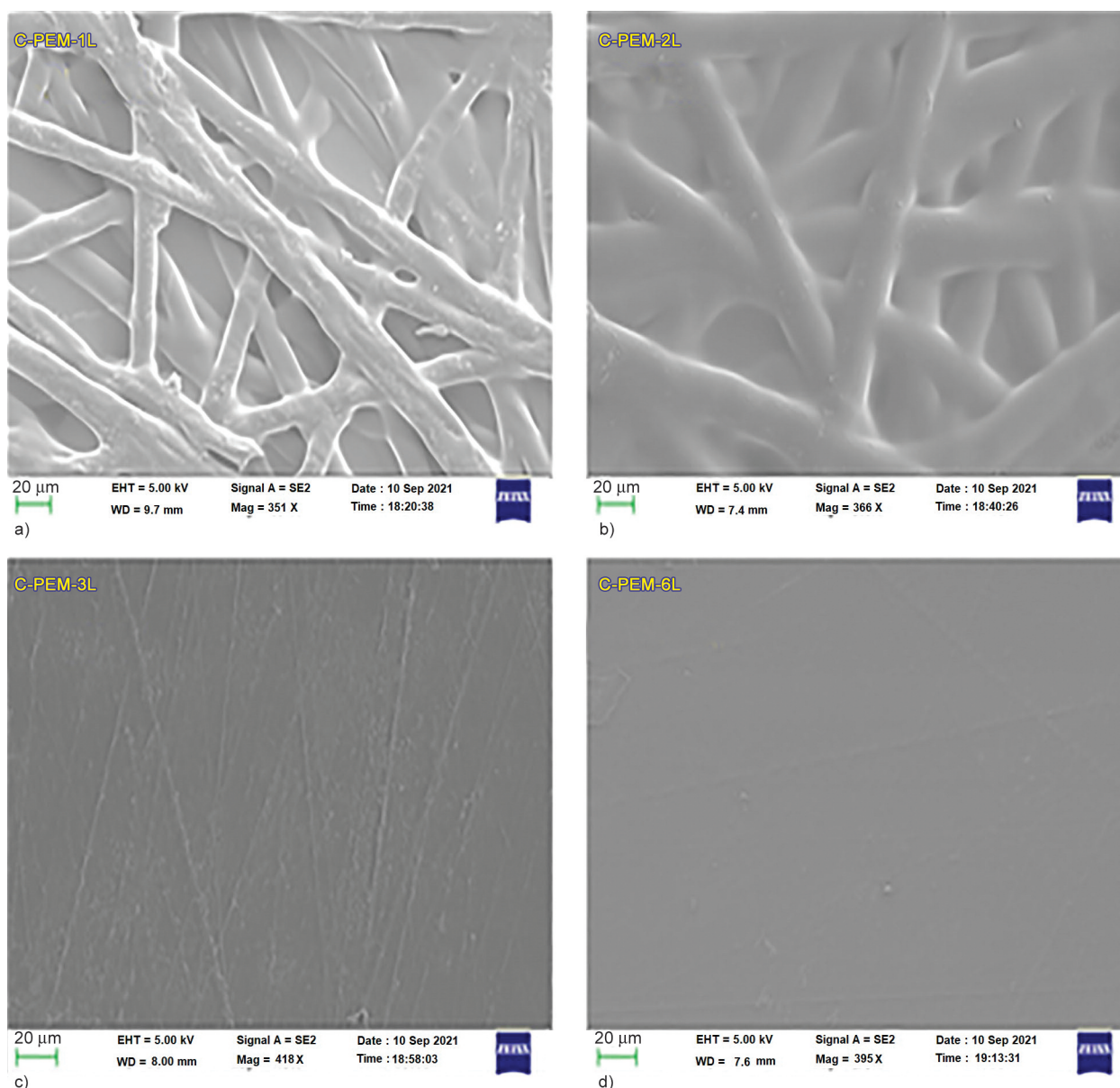

Figure 15. Surface topography of PVA-*co*-SSA/S-NWF-based composite PEMs. a) C-PEM-1L, b) C-PEM-2L, c) C-PEM-3L, d) C-PEM-6L.

Side views of the composite PEMs (Figure 16) were evaluated by examining the cross-sectional surface of the membranes after applying a gold-palladium conductive coating. As seen from the cross-sectional micrographs of the PEMs, the dip-coating technique formed a more uniform and thicker layer as the number of coating layers increased. It was further observed that the membranes having thicker layer coatings (C-PEM-3L and C-PEM-6L) showed dense structure morphology. Now, at the interface of S-NWF/ PVA-*co*-SSA, some micro-voids were observed, which were believed to be formed during the sample preparation (for SEM) upon fracturing in liquid nitrogen due to interfacial fiber/polymer debonding and fiber pull-out. This phenomenon of fiber pull-out can be attributed to weak interfacial bonding between sulfonated PP fibers of S-NWF and the impregnated PVA-*co*-SSA matrix, and this is not an inherent property of the PEMs. The relative distribution of the constituent elements present in C-PEM-6L was examined by the energy-dispersive X-ray spectroscopy (EDX), as presented in Figure 17. A uniform distribution of sulfur (S), oxygen (O), and carbon (C) elements throughout the PEM surface was observed from the elemental mapping (Figure 17c–7e). This further indicated the close packing of the polymer chains, resulting in the production of the observed dense morphology of the membrane.
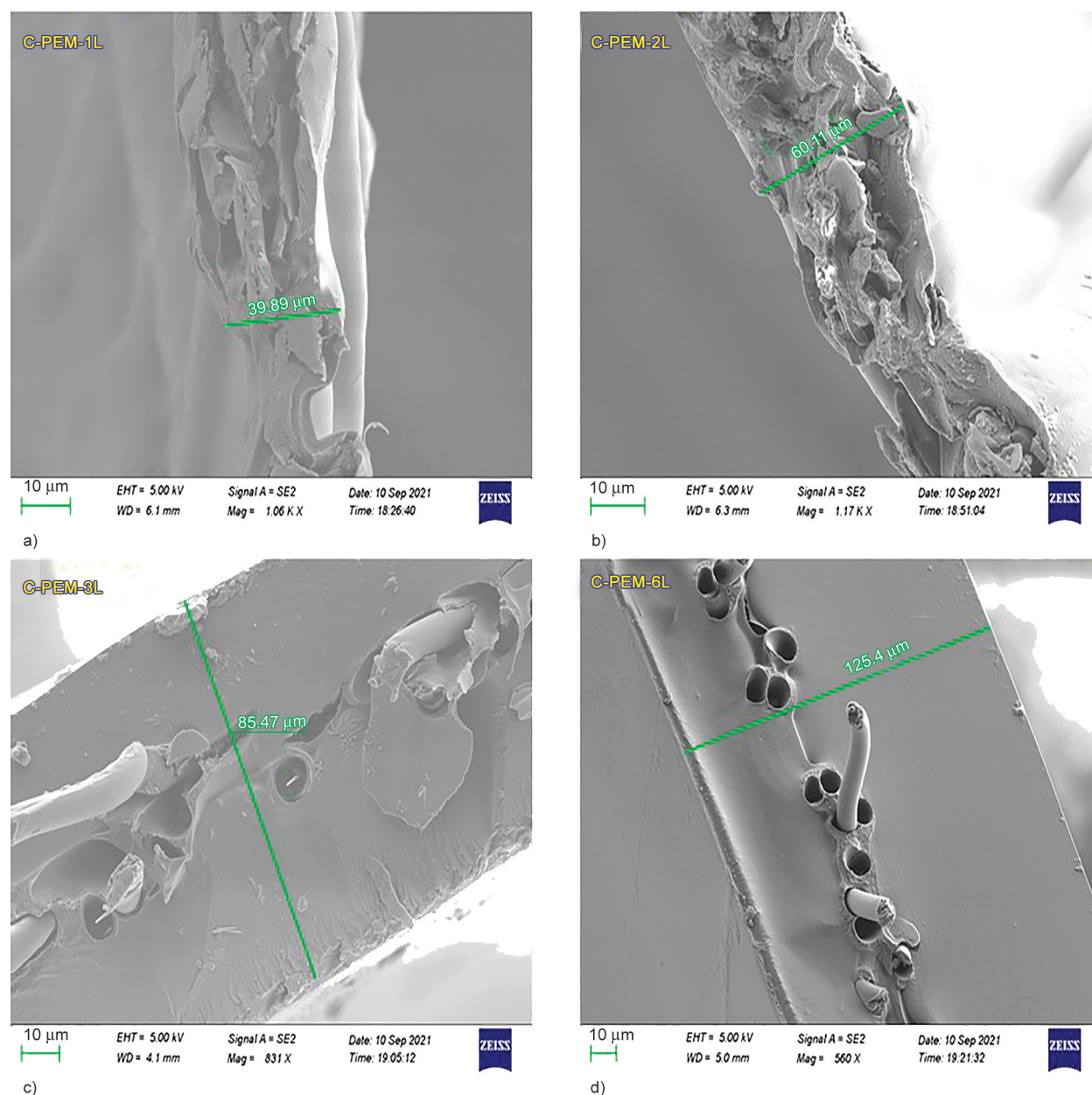

Figure 16. FE-SEM cross-sectional views of PVA-*co*-SSA/S-NWF-based composite PEMs. a) C-PEM-1L, b) C-PEM-2L, c) C-PEM-3L, d) C-PEM-6L.
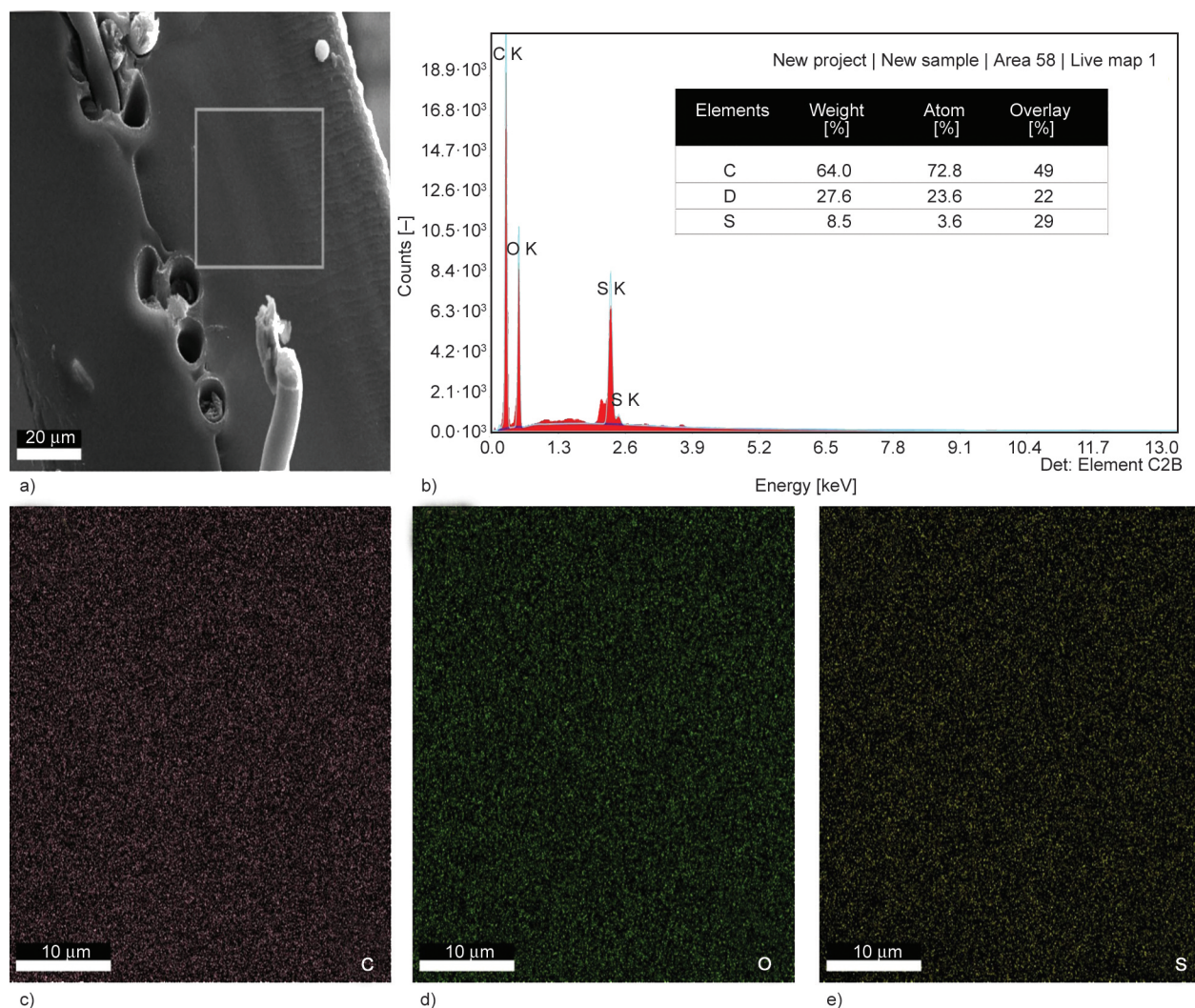
Figure 17. (a) FE-SEM images for a cross-sectional view of C-PEM-6L, (b) EDX analysis, and (c–e) elemental mapping for 'C', 'O', and 'S' in the C-PEM-6L surface.

3.9. DMFC performance

The fabricated composite PEMs based on PVA-*co*-SSA/S-NWF were tested in a single cell DMFC to evaluate their performance. For this purpose, the MEAs were fabricated using C-PEM-2L, C-PEM-3L and C-PEM-6L and assembled into a single-cell DMFC stack. The efficiency of the PEMs was determined at 60 °C. The polarization curves (*i–V*) obtained for all the membranes have been presented in Figure 18. The composite PEMs exhibited an open circuit potential (OCP) of about 0.6 V, which implies the low permeability of methanol through the membranes. The power density of the PEMs got increased with an increase in the number of coating layers, which was due to the observed improvements in proton conductivity, *IEC* and water uptake of the PEMs with increasing coating layer thickness. It was further observed that the PEM having 6 coating layers produced the highest peak power density of 62.32 W·m^{-2} and

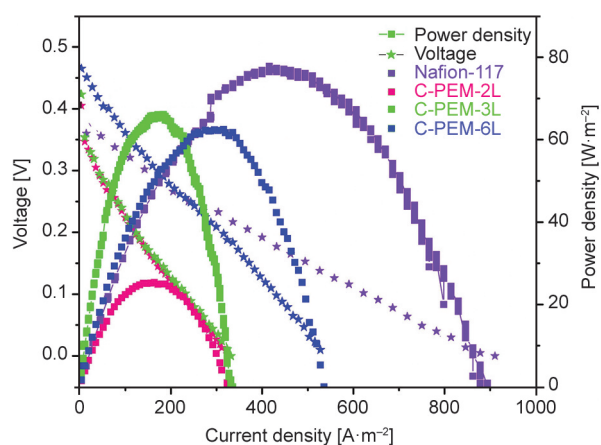**Figure 18.** The polarization curves of the DMFCs that were assembled with PVA-*co*-SSA/S-NWF-based composite membranes.

current density of 540 W·m^{-2}. In summary, the current density obtained from the DMFC, equipped with the robust composite C-PEM-6L, was acceptable,

and the resulting power density was moderately lesser than that of Nafion-117.

4. Conclusions

Herein, PP-NWF was successfully modified by the sulfonation process to induce ionic characteristics upon the incorporation of sulfonic acid groups. Water uptake and *IEC* of S-NWF were found to improve without appreciable loss in tensile strength. The reinforced composite membranes, obtained by impregnation (dip-coating) of S-NWF into PVA-*co*-SSA/GA solution, were found to possess uniform morphology and crosslinked structure. Crosslinking of PVA-*co*-SSA using GA was confirmed by FTIR, and the formation of dense morphology of the resulting membranes was viewed using SEM analysis. The various characteristics of PEMs, namely water-uptake, % swelling, methanol permeability, proton conductivity, PEM selectivity, thermal stability, and crystallinity, were analyzed for membranes possessing a varying number of crosslinked coating layers. All the composite PEMs showed lower methanol permeation than Nafion-117, as well as comparable proton conductivity. The optimized PEM (*i.e.*, C-PEM 6L) showed a maximum current density of 540 A·m^{-2} and peak power density of 62.32 W·m^{-2} in a single cell DMFC operated at 60 °C. Further, it is expected that the development of PEMs by applying the sequential layer of Nafion and PVA-*co*-SSA onto S-NWF, will result in a low methanol permeable membrane with increased power output in DMFC.

References

[1] Kolde J. A., Bahar B., Wilson M. S., Zawodzinski T. A., Gottesfeld S.: Advanced composite polymer electrolyte fuel cell membranes. Electrochemical Society Proceedings, **95**, 193–201 (1995).
https://doi.org/10.1149/199523.0193PV

[2] Penner R., Martin C.: Ion transporting composite membranes: I. Nafion-impregnated Gore-Tex. Journal of Electrochemical Society, **132**, 514–515 (1985).
https://doi.org/10.1149/1.2113875

[3] Shabanpanah S., Omrani A., Lakouraj M. M.: Fabrication and characterization of PVA/NNSA/GLA/nano-silica proton conducting composite membranes for DMFC applications. Designed Monomers and Polymers, **22**, 130–139 (2019).
https://doi.org/10.1080/15685551.2019.1626323

[4] Feng K., Tang B., Wu P.: Selective growth of MoS$_2$ for proton exchange membranes with extremely high selectivity. ACS Applied Materials and Interfaces, **5**, 13042–13049 (2013).
https://doi.org/10.1021/am403946z

[5] Pagidi A., Arthanareeswaran G., Seepana M. M.: Synthesis of highly stable PTFE-ZrP-PVA composite membrane for high-temperature direct methanol fuel cell. International Journal of Hydrogen Energy, **45**, 7829–7837 (2020).
https://doi.org/10.1016/j.ijhydene.2019.04.164

[6] Kausar A.: Fabrication and characteristics of poly(benzimidazole/fluoro/ether/siloxane/amide)/sulfonated polystyrene/silica nanoparticle-based proton exchange membranes doped with phosphoric acid. International Journal of Polymeric Materials and Polymeric Biomaterials, **64**, 184–191 (2015).
https://doi.org/10.1080/00914037.2014.936589

[7] Gonggo S. T., Bundjali B., Hariyawati K., Arcana I. M.: The influence of nano-silica on properties of sulfonated polystyrene-lignosulfonate membranes as proton exchange membranes for direct methanol fuel cell application. Advanced Polymeric Technology, **37**, 1859–1867 (2018).
https://doi.org/10.1002/adv.21844

[8] Yoo M., Kim M., Hwang Y., Kim J.: Fabrication of highly selective PVA-*g*-GO/SPVA membranes *via* crosslinking method for direct methanol fuel cells. Iconics, **20**, 875–886 (2014).
https://doi.org/10.1007/s11581-013-1026-7

[9] Gonzalez-Guisasola C., Ribes-Greus A.: Dielectric relaxations and conductivity of cross-linked PVA/SSA/GO composite membranes for fuel cells. Polymer Testing, **67**, 55–67 (2018).
https://doi.org/10.1016/j.polymertesting.2018.01.024

[10] Das G., Kang D., Yoon H. H.: A proton conducting composite membrane based on polyvinyl alcohol and polyaniline-intercalated graphene oxide. Journal of the Korean Physical Society, **74**, 384–388 (2019).
https://doi.org/10.3938/jkps.74.384

[11] Zakaria Z., Kamarudin S. K., Timmiati S. N., Masdar M. S.: New composite membrane poly(vinyl alcohol)/graphene oxide for direct ethanol–proton exchange membrane fuel cell. Journal of Applied Polymer Science, **136**, 46928 (2019).
https://doi.org/10.1002/app.46928

[12] Gil-Castell O., Santiago Ó., Pascual-Jose B., Navarro E., Leo T. J., Ribes-Greus A.: Performance of sulfonated poly(vinyl alcohol)/graphene oxide polyelectrolytes for direct methanol fuel cells. Energy Technology, **8**, 2000124 (2020).
https://doi.org/10.1002/ente.202000124

[13] Erkartal M., Usta H., Citir M., Sen U.: Proton conducting poly(vinyl alcohol) (PVA)/poly(2-acrylamido-2-methylpropane sulfonic acid) (PAMPS)/ zeolitic imidazolate framework (ZIF) ternary composite membrane. Journal of Membrane Science, **499**, 156–163 (2016).
https://doi.org/10.1016/j.memsci.2015.10.032

[14] Thakur V. K., Vennerberg D., Kessler M. R.: Green aqueous surface modification of polypropylene for novel polymer nanocomposites. ACS Applied Materials and Interfaces, **6**, 9349–9356 (2014).
https://doi.org/10.1021/am501726d

[15] Choi S., Kim J. R., Cha J., Kim Y., Premier G. C., Kim C.: Enhanced power production of a membrane electrode assembly microbial fuel cell (MFC) using a cost effective poly[2,5-benzimidazole] (ABPBI) impregnated non-woven fabric filter. Bioresource Technology, **128**, 14–21 (2013).
https://doi.org/10.1016/j.biortech.2012.10.013

[16] Grandi S., Mustarelli P., Carollo A., Tomasi C., Quartarone E., Magistris A.: PWA doped SiO_2 PEG hybrid materials of class II. Material Science and Applications, **1**, 285–291 (2010).
https://doi.org/10.4236/msa.2010.15042

[17] Bahar B., Hobson A. R., Kolde J. A.: Integral composite membrane. U.S. Patent 5599614, USA (1995).

[18] Bahar B., Hobson S. R., Kolde J. A., Zuckerbrod D.: Ultra-thin integral composite membrane. U.S. Patent 5547551, USA (1996).

[19] Vielstich W., Gasteiger H. A., Yokokawa H.: Handbook of fuel cells: Advances in electrocatalysis, materials, diagnostics and durability. Wiley, Chirchester (2009).

[20] Liu W., Ruth K., Rusch G.: Membrane durability in PEM fuel cells. Journal of New Materials for Electrochemical Systems, **4**, 227–231 (2001).

[21] Collier A., Wang H., Yuan X. Z., Zhang J., Wilkinson D. P.: Degradation of polymer electrolyte membranes. International Journal of Hydrogen Energy, **31**, 1838–1854 (2006).
https://doi.org/10.1016/j.ijhydene.2006.05.006

[22] Chen L-C., Yu T. L., Lin H-L., Yeh S-H.: Nafion/PTFE and zirconium phosphate modified Nafion/PTFE composite membranes for direct methanol fuel cells. Journal of Membrane Science, **307**, 10–20 (2008).
https://doi.org/10.1016/j.memsci.2007.03.008

[23] Pandey J., Seepana M. M., Shukla A.: Zirconium phosphate based proton conducting membrane for DMFC application. Internatinal Journal of Hydrogen Energy, **40**, 9410–9421 (2015).
https://doi.org/10.1016/j.ijhydene.2015.05.117

[24] Cheng G., Li Z., Ren S., Han D., Xiao M., Wang S., Meng Y.: A robust composite proton exchange membrane of sulfonated poly(fluorenyl ether ketone) with an electrospun polyimide mat for direct methanol fuel cells application. Polymers, **13**, 523 (2021).
https://doi.org/10.3390/polym13040523

[25] Vicente A. I., Ferreira A. E., Ribeiro M. R.: New route to functional polyolefins: Sulfonation of poly[ethylene-*co*-(5,7-dimethylocta-1,6-diene)] and evaluation of properties. Polymer International, **66**, 1005–1012 (2017).
https://doi.org/10.1002/pi.5348

[26] Choudhury R. R., Gohil J. M., Mohanty S., Nayak S. K.: Synthesis and characterization of novel functional poly (vinyl alcohol-*co*-styrene sulfonic acid) copolymers. International Journal of Polymer Analysis and Characterization, **24**, 334–345 (2019).
https://doi.org/10.1080/1023666X.2019.1596367

[27] Kovačič S., Žagar E., Slugovc C.: Strength *versus* toughness of emulsion templated poly(dicyclopentadiene) foams. Polymer, **169**, 58–65 (2019).
https://doi.org/10.1016/j.polymer.2019.02.045

[28] Cruz Zavala A.S., Escobar-Barrios V. A.: Sulfonation of a flexible and unexpected electrically conductive polysulfone and its performance in perovskites solar cells. Materials Today Chemistry, **16**, 100212 (2020).
https://doi.org/10.1016/j.mtchem.2019.100212

[29] Kundu P. P., Dutta K., Kumar P., Bharti R. P., Kumar V., Kundu P. P.: Polymer electrolyte membranes for microbial fuel cells: Part A. Nafion-based membranes. in 'Progress and recent trends in microbial fuel cells' (eds.: Kundu P. P., Dutta K.) Elsevier, Amsterdam, 47–72 (2018).

[30] Colpan C. O., Nalbant Y., Ercelik M.: Fundamentals of fuel cell technologies. in 'Comprehensive energy systems' (ed.: Dincer I.) Elsevier, Cambridge, Vol 4, 1107–1130 (2018).

[31] Kim D., Park H. B., Rhim J. W., Lee Y. M.: Preparation and characterization of crosslinked PVA/SiO_2 hybrid membranes containing sulfonic acid groups for direct methanol fuel cell applications. Journal of Membrane Science, **240**, 37–48 (2004).
https://doi.org/10.1016/j.memsci.2004.04.010

[32] Lin J-H., Pan Y-J., Liu C-F., Huang C-L., Hsieh C-T., Chen C-K., Lin Z-I., Lou C-W.: Preparation and compatibility evaluation of polypropylene/high density polyethylene polyblends. Materials, **8**, 8850–8859 (2015).
https://doi.org/10.3390/ma8125496

[33] Krylova V., Dukštienė N.: Synthesis and characterization of Ag_2S layers formed on polypropylene. Journal of Chemistry, **2013**, 987879 (2013).
https://doi.org/10.1155/2013/987879

[34] Tada H., Ito S.: Conformational change restricted selectivity in the surface sulfonation of polypropylene with sulfuric acid. Langmuir, **13**, 3982–3989 (1997).
https://doi.org/10.1021/la960885l

[35] Kaneko M., Sato H.: Sulfonation of poly(propylene) films with fuming sulfuric acid. Macromolecular Chemistry and Physics, **206**, 456–463 (2005).
https://doi.org/10.1002/macp.200400312

[36] Dang H-S., Kim D.: Cross-linked poly(arylene ether ketone) membranes sulfonated on both backbone and pendant position for high proton conduction and low water uptake. Journal of Power Sources, **222**, 103–111 (2013).
https://doi.org/10.1016/j.jpowsour.2012.08.079

[37] Gohil J., Karamanev D. G.: Novel pore-filled polyelectrolyte composite membranes for cathodic microbial fuel cell application. Journal of Power Sources, **243**, 603–610 (2013).
https://doi.org/10.1016/j.jpowsour.2013.06.001

[38] Rudra R., Kumar V., Kundu P. P.: Acid catalysed crosslinking of poly vinyl alcohol (PVA) by glutaraldehyde: Effect of crosslink density on the characteristics of PVA membranes used in single chambered microbial fuel cells. RSC Advances, **5**, 83436–83447 (2015).
https://doi.org/10.1039/C5RA16068E

[39] Dutta K., Das S., Kundu P. P.: Low methanol permeable and highly selective membranes composed of pure and/or partially sulfonated PVdF-*co*-HFP and polyaniline. Journal of Membrane Science, **468**, 42–51 (2014).
https://doi.org/10.1016/j.memsci.2014.05.049

[40] Dutta K., Kumar P., Das S., Kundu P. P.: Utilization of conducting polymers in fabricating polymer electrolyte membranes for application in direct methanol fuel cells. Polymer Reviews, **54**, 1–32 (2014).
https://doi.org/10.1080/15583724.2013.839566

[41] Gomaa M. M., Hugenschmidt C., Dickmann M., Abdel-Hady E. E., Mohamed H. F. M., Abdel-Hamed M. O.: Crosslinked PVA/SSA proton exchange membranes: Correlation between physiochemical properties and free volume determined by positron annihilation spectroscopy. Physical Chemistry Chemical Physics, **20**, 28287–28299 (2018).
https://doi.org/10.1039/C8CP05301D

[42] Dutta K., Das S., Kundu P. P.: Highly methanol resistant and selective ternary blend membrane composed of sulfonated PVdF-*co*-HFP, sulfonated polyaniline and nafion. Journal of Applied Polymer Science, **133**, 43294 (2016).
https://doi.org/10.1002/app.43294

[43] Choudhury R. R., Gohil J. M., Dutta K.: Poly(vinyl alcohol)-based membranes for fuel cell and water treatment applications: A review on recent advancements. Polymer for Advanced Technology, **32**, 4175–4203 (2021).
https://doi.org/10.1002/pat.5431

[44] Chrissopoulou K., Anastasiadis S. H.: Polyolefin/layered silicate nanocomposites with functional compatibilizers. European Polymer Journal, **47**, 600–613 (2011).
https://doi.org/10.1016/j.eurpolymj.2010.09.028